

pubs.acs.org/JPCL Letter

Plumbing Potentials for Molecules with Up To Tens of Atoms: How to Find Saddle Points and Fix Leaky Holes

Ankit Pandey and Bill Poirier*



Cite This: J. Phys. Chem. Lett. 2020, 11, 6468-6474



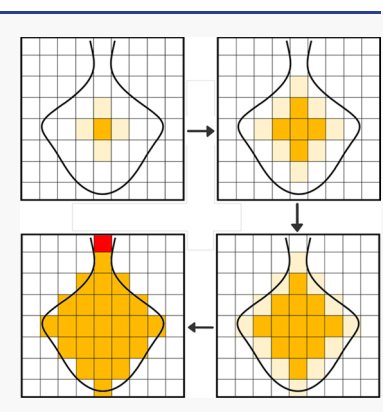
ACCESS

III Metrics & More

Article Recommendations

Supporting Information

ABSTRACT: Potential energy surfaces (PESs) play an indispensable role in molecular dynamics but are notoriously difficult to flesh out properly in large-dimensional spaces. In particular, the undetected presence of PES holes, i.e., unphysical saddle points beyond which the potential energy drops arbitrarily, can have devastating effects on both classical and quantum dynamics calculations. In this study, the *Crystal* algorithm is developed as a tool for efficiently and accurately finding PES holes, as well as legitimate saddle points, even in very large-dimensional configuration spaces. The approach is applied to three large-dimensional PESs for molecular systems of current interest: uracil, naphthalene, and formic acid dimer. Low-lying PES holes are discovered and located for the first two systems—including naphthalene, for which no holes were previously suspected, to the best of our knowledge. Likewise, the double-well, double-proton-transfer isomerization saddle point for formic acid dimer is also located.



ncreasingly, all-atom dynamical calculations are used to simulate larger molecular systems. Despite progress, such calculations remain challenging, whether performed classically, quantum mechanically, or via some intermediate approximate quantum strategy. 1-3 For large systems, potential energy surfaces (PESs) are often eschewed entirely, in favor of "direct" dynamics.4 This approach offers many advantages but has the disadvantage that gradients and Hessians must generally be computed "on the fly," which can be expensive. Alternatively, recent advances in "automatic" PES construction⁵⁻⁷ have proven to be remarkably effective, even for large-dimensional spaces, confirming that explicit PESs will continue to play a vital role in the foreseeable future of dynamics. This is all the more likely, given the increasingly important role of artificial neural networks and other machine learning techniques across all facets of science and engineering, including PES construction. 8-11

Short of a full-fledged dynamical understanding, it is desirable to at least know all of the relevant reaction pathways of a chemical system, which has been deemed nothing less than "the most important task in the theoretical study ... of chemical reactions". This, too, is an extreme challenge in large-dimensional spaces, whose "bottleneck" operation is the determination of all relevant transition state structures (i.e., first-order saddle points). To this end, a great many numerical optimization techniques, generally requiring at least gradient calculations, have been developed and applied over the years. Paughly speaking, these include interpolation methods Roughly speaking, these include interpolation methods and nudged elastic band that seek to find the saddle point between two known reactant and product

geometries (generally minima) and local methods ^{12,13,15,19} (e.g., gradient norm minimization ¹⁵ and Newton–Raphson ^{15,19}) designed to "hone in" on the exact saddle point starting from a nearby "guess" geometry lying within the convergence/trust radius.

Both types of optimization methods generally suffer from the limitation that a good set of coordinates, and at least one geometry, must be known ahead of time, through chemical intuition or other means. 12,13,15 More recent—and ambitious—efforts start from a given local minimum and/or seek to find all relevant saddle points automatically. 12-15,20-22 One particularly effective approach is to expand outward in a series of (harmonically) isoenergetic shells, whose (true) energetic minima¹³ or anharmonic downward distortions point out the paths toward saddle points and other minima. 12-14 Such methods have been used to find full-dimensional reaction pathways for molecules with as many as 12 atoms (with parallelization). 12 Even more importantly, they predicted an unexpected new mechanism for NO3 photolysis via "excited state roaming", which was later confirmed experimentally, 23,24 thus demonstrating the significance for experimental as well as theoretical chemical science.

On the other hand, and despite much progress, there are no general optimization methods for first-order saddle points that

Received: May 10, 2020 **Accepted:** July 20, 2020 **Published:** July 20, 2020





are guaranteed to work¹⁵—certainly not, say, for finding the lowest-lying saddle point, then the next lowest-lying saddle point, etc. Such a guarantee would require "a mapping of the whole surface", which has been called "impossible for more than three or four variables".¹⁵ According to the conventional wisdom, this is because the size of the space that must be explored increases exponentially with the system dimensionality, *D*. This belief explains why the mapping approach has been eschewed for decades, in favor of the bewildering array of complex and heuristical optimization strategies currently in use.

The *Crystal* method presented here differs from all previous methods in that it is indeed a mapping approach, and therefore offers a guaranteed strategy for finding saddle points, in principle. It is also fully automatic, conceptually very simple, and not especially sensitive to the choice of coordinates. *Crystal* is also numerically efficient, even at large values of D (evidently up to tens of atoms). This is because in reality, PES complexity scales only polynomially rather than exponentially for most molecules. Of course, pathological counterexamples can be devised; moreover, there are some caveats pertaining to the size of the discretization step. Nevertheless, we demonstrate in this Letter, through realistic molecular examples with up to 18 atoms (D = 48), that such a mapping approach is indeed viable in practice and should therefore serve as a useful complement to the optimization methods already in play.

Although *Crystal* can in principle be applied in both constructed PES and "on-the-fly" contexts, in this Letter, we consider only the former. In particular, we concentrate mainly on the highly challenging problem of finding PES holes—i.e., unphysical saddle points, beyond which the minimum energy path descends arbitrarily (e.g., to negative infinity). Constructed PESs that take the form of a truncated Taylor series, anharmonic force field (AFF) are especially prone to holes, especially for large values of *D*. Increasing the order of the polynomial expansion can help, ^{14,28} as can nonpolynomial strategies (e.g., "Morsification"²⁹). In truth, however, these strategies offer no guarantee of success, as this would be tantamount to knowing the saddle points *a priori*. Indeed, finding PES hole saddle points is all the more difficult, because (a) chemical intuition offers no indication as to where they might be located and (b) from a dynamical standpoint, it is essential to find the lowest-lying holes first.

Consideration (b) arises because the lowest-lying PES holes impose an artificial upper limit on the energies for which reliable dynamical calculations can be performed. In quantum dynamics calculations, holes can manifest as very slow convergence, spurious energy levels, or even subtler effects, as a result of which, it can be difficult to even know that one has entered a hole region. It appears that PES holes are quite common at large values of *D*, which is also where they become the most difficult to detect and fix! Despite best efforts by PES developers to do this "by hand" (e.g., by adding new *ab initio* points and refitting), it is clear that some kind of PES holefinder tool—one that is accurate, efficient, reliable, and automated—is very badly needed for dealing with this increasingly troublesome nuisance.

Our *Crystal* code^{26,30} has been developed to serve as just such a resource. Originally designed for fleshing out classically allowed regions of phase space,³⁰ *Crystal* has been recently "retooled" to serve as a PES saddle point and hole finder, by mapping out configuration space (i.e., the space of all

geometries) instead of phase space. For the study presented here, three specific molecular applications were chosen: uracil, naphthalene, and formic acid dimer. These represent some of the largest molecules for which full-dimensional PESs are available, and quantum dynamics calculations have been attempted. In addition to rather large system dimensionalities ($D=30,\ D=48,\$ and $D=24,\$ respectively), the corresponding PES functions themselves exhibit a commensurate complexity. Our goal in this Letter is not only to analyze the PESs for these complicated, important systems in their own right, but also to evaluate Crystal's performance as a mapping-based saddle point finder, in the context of both holes and legitimate saddle points, when pushed to the limits of real-world PESs.

 $Uracil^{31}$ [$C_4H_4O_2N_2$ (Figure 1)] is one of the four nucleobases in the nucleic acid of RNA. It has a role in the



Figure 1. Molecular structures for uracil (left), naphthalene (middle), and formic acid dimer (right).

synthesis of many enzymes and can also be used for drug delivery. Hence, it has been the subject of intense interest in biology, evolution, and pharmaceutics. With 12 atoms, uracil has a total of D = 30 vibrational modes. Several years ago, a full-dimensional AFF PES was developed by Krasnoshchekov et al.³² The uracil PES has a total of 7796 AFF monomial terms, provided up to quartic order.³² This is an unusually large number, in comparison to those of typical quartic AFF PESs of comparable dimensionality. For example, the benzene PES (also D = 30), as used in several recent studies, $^{26,33-35}$ has only around 500 terms. The comparatively much larger number in the case of uracil indicates higher anharmonicity and coupling for this system, and a higher probability of holes. Thomas et al.²⁷ (correctly) inferred the presence of a low-lying hole for this PES; however, they did not locate its position. The uracil PES thus serves as an interesting test case for

Best known as the main ingredient in traditional mothballs, naphthalene $[C_{10}H_8 \text{ (Figure 1)}]$ is also the smallest polycyclic aromatic hydrocarbon (PAH).³⁶ It has been the subject of spectroscopic studies, owing to the role of PAHs as pollutants. Despite its 18 atoms and D=48 dimensions, a PES was developed as early as 2007 by Cané et al.³⁷ The naphthalene PES is also a quartic AFF and, as such, is very likely to have holes. On the other hand, it consists of a substantially smaller (but still very large) number of terms (4191) than the uracil PES, despite the much larger dimensionality. This suggests significantly less anharmonicity and coupling for naphthalene than for uracil, which is also consistent with chemical intuition.

Even in the gas phase, formic acid dimer $[(CH_2O_2)_2$ (Figure 1)] is the most prevalent form of this smallest of the carboxylic acids. This is due to its propensity to form hydrogen bonds, of which even the (cyclic) dimer has two. Moreover, the dimer dynamics are highly interesting, in that simultaneous exchange of the two hydroxyl H atoms gives rise to a second equivalent structure. This double-well, double-proton-transfer isomerization thus presents a highly challenging test case, ideal for

evaluating *Crystal* in the context of finding legitimate saddle points. We use the recent, full-dimensional PES of Qu and Bowman.³⁹

The uracil and naphthalene PESs described above were the subject of a recent quantum dynamics study by Thomas et al., 27 who computed vibrational energy levels near the bottom of the dynamically relevant spectrum. Although only the lowest-lying states were considered (i.e., within ~1200 and ~1026 cm⁻¹ of the ground state for uracil and naphthalene, respectively), the authors could nevertheless infer the presence of an unphysical hole in the uracil PES, due to spurious energy eigenvalues. They then undertook significant effort to modify the PES, which was originally developed by a different group,³ to obtain a reasonably close alternative without holes. Although unsuccessful in eliminating all holes (without adversely impacting the resultant computed energy levels), the authors were at least able to mitigate hole damage in the low-lying spectral region considered. In the case of naphthalene, the authors mentioned above saw no direct evidence for the existence of a PES hole, so they used the original \mbox{PES}^{37} without modification. This led to no apparent ill effects—but of course, in and of itself, this is no guarantee that there is not a low-lying PES hole for this system, as well. In any event, the vignette described above serves to underscore the pressing need for fast and reliable hole-finding tools such as Crystal that can be applied prior to performing expensive quantum dynamics calculations.

The use of *Crystal* to find both PES holes and legitimate saddle points proceeds as follows.

- (1) Choose a low-energy initial point (e.g., the global minimum geometry) for which the PES value, V, is less than some chosen energy cutoff, $V_{\rm cut}$.
- (2) Run *Crystal* to "grow" a set of lattice grid points for which $V < V_{\text{cut}}$ until all N such grid points have been found.
- (3) If N diverges (or otherwise grows very large), there is a saddle point below $V_{\rm cut}$: set $V_{\rm cut2} = V_{\rm cut}$; reduce $V_{\rm cut}$ until N no longer diverges; and set $V_{\rm cut1} = V_{\rm cut}$.
- (4) Otherwise, there is no saddle point below V_{cut} : set $V_{\text{cut}1} = V_{\text{cut}}$; increase V_{cut} until N diverges; and set $V_{\text{cut}2} = V_{\text{cut}}$.
- (5) "Divide and conquer" the interval between $V_{\text{cut}1}$ and $V_{\text{cut}2}$ until the saddle point region is narrowly identified.
- (6) Use standard optimization techniques (nudged elastic band, ¹⁶ Newton–Raphson, ¹⁹ and gradient norm minimization ¹⁵) to pinpoint the precise location of the saddle point.

A more detailed overview is provided below. For a complete exposition, see the companion paper, ²⁶ which also provides the complete *Crystal* source code and user's manual. Updated versions of the latter are also available from the authors on request. These include refinements that have since been made to the original code, mostly pertaining to the treatment of second-order saddle points and non-zero gradient norm minima, as are also described in this Letter.

The basic operation of the *Crystal* mapping algorithm is conceptually straightforward. First, we define an infinite rectlinear lattice of grid points, spanning the entire configuration space, $(Q_1, Q_2, ..., Q_D)$, where the Q_i denote individual vibrational modes or internal coordinates. For each Q_i , there is a natural choice of lattice spacing (as discussed in detail in the companion paper²⁶), in terms of which all grid point locations become integer-valued vectors with D components.

Without loss of generality, we take the initial point from step 1 above as the Q_i coordinate origin, (0, 0, ..., 0). This point is

known to lie within the configuration space region of interest, so that $V(0,0,...,0) < V_{\rm cut}$. Starting from this initial point, all nearest neighbor points in all D directions are then considered—i.e., the points $(0,0,...,Q_i=\pm 1,...,0,0)$, for all $1 \le i \le D$. There are a total of 2D such nearest neighbor points. For each of these, $V(Q_1,Q_2,...,Q_D)$ is evaluated and compared to $V_{\rm cut}$. Those points that satisfy $V(Q_1,Q_2,...,Q_D) < V_{\rm cut}$ are combined with the initial point to form the "current set". In each subsequent iteration, the nearest neighbor points for the current set are determined. If these are new points, then $V(Q_1,Q_2,...,Q_D)$ is evaluated; if $V < V_{\rm cut}$ then these points are added to the new current set. Iterations proceed until no new points are added to the current set, which will happen eventually, provided that the region of interest is bounded.

The simple description given above suggests a computational (CPU) scaling of DN, in terms of both CPU effort and memory (note that N itself has an implicit dependence on D, which is where the overall polynomial scaling comes from). In practice, there are many issues that make efficient numerical implementation a challenge. For example, at each iteration, it is necessary to check nearest neighbor points against all current set points, to avoid duplication and redundant effort. A naive search might thus lead to DN² scaling of CPU effort—which, assuming say $N \approx 10^9$, becomes unfeasible. Of course, standard sort algorithms, based on binary tree structures, can be used to reduce the scaling to DN log N. These typically require extensive use of pointers, however, which gives rise to very substantial CPU overhead (in terms of both effort and memory). Alternatively, pointer-free array-based approaches may also be used, but generally at the expense of having to move vast amounts of data to accommodate the growing binary tree, which is even more expensive.

Crystal exploits an alternate strategy that provides the "best of both worlds"—i.e., using simple arrays (mostly containing just short integers) instead of pointers, yet implemented in such a manner that growing a binary tree does not require any copying of data. As a consequence, $DN \log N$ scaling of CPU effort, and DN scaling of CPU memory, are achieved with minimal overhead. (Note the linear D scaling, reminiscent of gradient-based optimization methods.) The method has been found to be extremely reliable and efficient, with typical execution times (for a single $V_{\rm cut}$ value) on the order of seconds 26

For bound molecular systems, N is guaranteed to be finite provided that $V_{\rm cut}$ lies below the first dissociation threshold, assuming that $V(Q_1, Q_2, ..., Q_D)$ is well-behaved. If, instead, a numerical PES happens to have an unphysical hole saddle point lying below the true dissociation threshold (and also below $V_{\rm cut}$), then N will grow indefinitely, in principle without limit. In practice, some very large upper limit $N_{\rm max}$ is chosen, such that when N reaches $N_{\rm max}$, Crystal stops and reports a hole. Through the "winnowing" described in step 5 above, it then becomes possible to narrow the hole saddle point region down to a single grid point (modulo symmetry considerations). We call this the "lattice hole point".

We next briefly address how our method is applied to find legitimate saddle points, i.e., the primary bottleneck in identifying reaction pathways. For dissociation pathways, the procedure is identical to that used for finding hole saddle points as described above. For isomerization pathways, the situation is similar: starting from the first isomer well, once $V_{\rm cut}$ reaches the transition state energy, there will be a sudden but finite jump in N, as the second well region suddenly becomes

available. By monitoring such sudden jumps in N, we can identify and locate legitimate isomerization saddle points.

After finding the lattice hole point using Crystal, several strategies may then be used to "hone in" on the precise location of the nearby saddle point itself. A nudged elastic band approach could be used, 16 although with the initial point chosen as the second end point, this might not be very efficient (and no other choice would be "black box"). A local method is generally preferable, with Newton-Raphson offering quadratically fast convergence, but also requiring Hessian evaluations. 19 Alternatively, we have employed the simple gradient norm minimization strategy, based on the magnitude of the local force vector, or norm of the PES gradient. This approach has been found to work quite well, despite its small radius of convergence, because of the proximity of the lattice hole point to the saddle point. 15,26 However, because it is not based on energy per se, it can sometimes converge to higher-lying "second-order saddle points" (two negative Hessian eigenvalues, instead of one), or even to gradient norm minima for which the gradient itself is non-zero. These situations were indeed observed for the molecules of this study. Consequently, when using gradient norm minimization, once the minimum is located, we ensure first that the PES gradient is in fact zero and second that the corresponding Hessian has exactly one negative eigenvalue.

In its role as both a PES hole finder and a legitimate transition state finder, *Crystal* would be much more valuable if it could find multiple saddle points in increasing energetic order, instead of just the lowest-lying one as described above. We have built such functionality into our code, through a procedure we call hole plugging, reminiscent of iterative optimization and elimination.¹² The idea is simple: once a lattice hole point is located, it is thereafter permanently "tagged," so that if and when it next appears in the current set of a subsequent *Crystal* execution, its nearest neighbor points are precluded from consideration. In practice, we find it convenient (but not necessary) to employ a refinement known as "cubic plugs", whose detailed explanation is reserved for the companion paper.²⁶

We return now to a discussion of the specific molecular applications, starting with uracil. The first step is to choose the lattice spacings. These are based on the harmonic frequencies, ²⁶ taken from the CCSD(T)-based values of Puzzarini et al. ⁴⁰ (Table S1). As for the anharmonic terms, their comparatively large number implies substantial CPU effort needed for each PES function evaluation, irrespective of the fact that a great many such PES evaluations might be required in such a large dimensional space.

Using *Crystal*, a low-lying hole was indeed identified and located in the uracil PES. For this hole, the $V_{\rm cut}$ interval in step 5 above was winnowed down to a $V_{\rm cut1}$ of 5348.09 cm⁻¹ and a $V_{\rm cut2}$ of 5348.11 cm⁻¹. This revealed a lattice hole point lying at the configuration labeled "Lattice Hole Point 1" in Table S3. Remarkably, the largest, $V_{\rm cut1} = 5348.09$ cm⁻¹, calculation above required <30 s of CPU time, running on a single core of the Quanah cluster at the Texas Tech University High Performance Computing Center. CPU memory requirements (<2 MB) were also remarkably minimal.

From the Lattice Hole Point 1 configuration of Table S3, we see that reaching the lowest-lying uracil hole region requires the simultaneous displacement of nine separate Q_i coordinates. Such a PES hole would be almost impossible to locate "by hand" (i.e., via plots of PES slices taken two or three

coordinates at a time) and also presents a challenge for optimization methods. Nevertheless, a total of only 22822 lattice grid points (N) were found to lie below this hole, which is not very many, given the dimensionality. For D=30, a PES hole with such a small N value may be expected to have severe dynamical repercussions. On the other hand, because our algorithm scales as $N \log N$, this small N value also helps explain why Crystal was able to find the hole so quickly.

Starting from Lattice Hole Point 1, gradient norm minimization was used in our initial attempt to find the corresponding hole saddle point. However, this led to a minimum with a non-zero gradient. From here, though, it was straightforward to find the true saddle point, following a minimum-energy path-type procedure. The results are presented in Table S3. Note that the uracil hole saddle point lies only 720.241 cm⁻¹ above the global minimum! It is thus no surprise that Thomas et al. encountered severe problems.²⁷ This energy is also much lower than the corresponding lattice hole point energy. This situation is typical for large-dimensional spaces and underscores the importance of finding the saddle point explicitly, once the nearby lattice hole point has been properly identified via *Crystal*.

Having precisely identified the hole saddle point, we can visually observe the hole behavior, via a one-dimensional plot of the PES, taken along a path from the global minimum, through the hole saddle point, and out into the hole region. Such a "reaction profile" plot is presented in Figure 2, for the

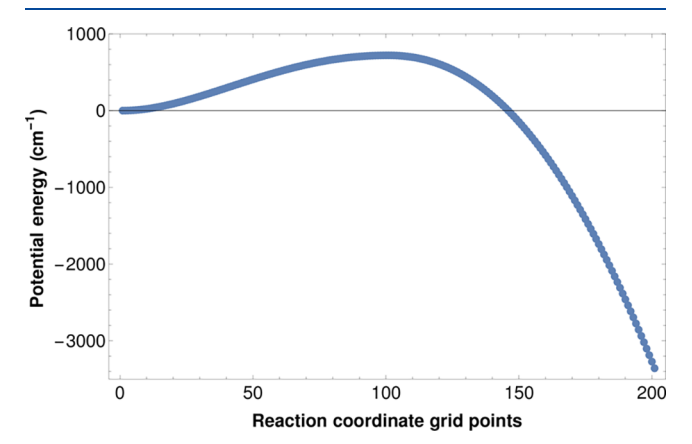


Figure 2. "Reaction profile" plot for the uracil PES of Krasnoshchekov et al. ³² The origin corresponds to the global minimum geometry, whereas the 100th point corresponds to the hole saddle point geometry, located a mere 720.241 cm⁻¹ above the minimum. Between the points, the reaction path is taken to be the straight line segment connecting the origin and the hole saddle point. Beyond the latter, the reaction path extends in the direction of the saddle point Hessian eigenvector with a negative eigenvalue. In this regime, the plot shows a monotonic descent toward negative infinity, the hallmark of a PES hole.

lowest-lying uracil PES hole. Beyond the saddle point, the hole behavior is quite glaring. Note also that in addition to being very low-lying, this hole appears to be quite broad, in the sense that it does not disappear under significant perpendicular mode displacements from the saddle point. One indication of this is the rather large difference between the lattice hole and saddle point configurations as presented in Table S3. Another indication is what occurs when the hole is "plugged", as described below.

Using a previously described notation, 26 a rather large "cubic plug" was inserted around Lattice Hole Point 1 of the uracil PES. Running *Crystal* again, we discovered a new lattice hole point. Lattice Hole Point 2 (as presented in Table S3) corresponds to a significantly higher PES energy ($V_{\rm cut}$ between 6985.76 and 6985.78 cm $^{-1}$). However, the similarity of the two lattice hole point configurations suggests that they in fact belong to the same broad hole. This hypothesis was confirmed via gradient minimization, etc., starting from Lattice Hole Point 2, which led to exactly the same hole saddle point as for Lattice Hole Point 1.

The D = 48 normal mode frequencies for naphthalene are listed in Table S2. As discussed, the naphthalene PES is far less anharmonic than for uracil, suggesting it is less likely to have a low-lying hole.²⁷ However, Crystal tells a different story. In particular, our calculations have revealed the existence of a naphthalene PES lattice hole point, at the configuration listed in Table S4. Note that "only" six modes are now coupled (displaced), rather than nine. Even so, the corresponding lattice hole point energy is larger than for uracil—i.e., $V_{\rm cut}$ between 6932.5 and 6933 cm⁻¹. A total of $N \approx 3.6$ million grid points lie below this hole. This is a much larger N value than for uracil, reflecting the larger D and V_{cut} values of naphthalene. The larger N leads to substantially greater CPU effort, despite the somewhat simpler PES. In particular, the largest $V_{\rm cut1}$ calculation for naphthalene required 2 h on a single CPU core of the Quanah cluster. This is still remarkably inexpensive, given the complexity of the problem.

Starting from the naphthalene lattice hole point described above, gradient norm minimization, etc., were again applied, to determine the location of the corresponding hole saddle point, given in Table S4. This point lies 2483.050 cm⁻¹ above the PES minimum—much higher than for uracil, but still a "low-lying" PES hole, potentially capable of inflicting harm on dynamical calculations. This is evidently not the case for the study of Thomas et al.; however, knowing for sure would require modifying the PES, so as to remove this newly discovered hole, or push it to a higher energy. In any event, the naphthalene hole can be clearly seen in Figure 3, where it is depicted graphically in a "reaction profile" plot.

To test the limits of the methodology still further, we also considered what happens when the naphthalene hole is "plugged". Again, a cubic plug was inserted; however, this time the effect was to "stop the leak". More specifically, $V_{\rm cut}$

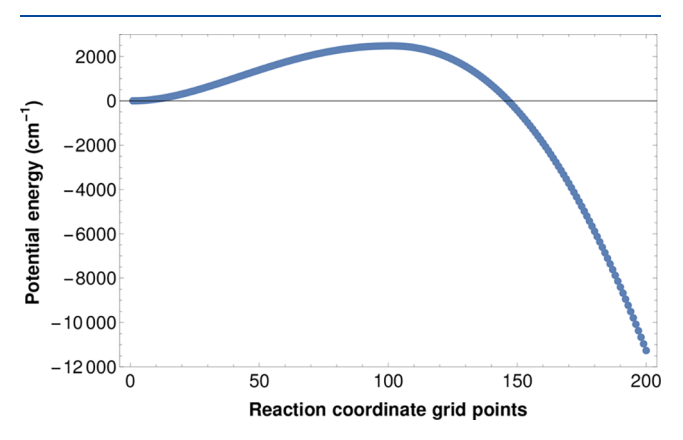


Figure 3. "Reaction profile" plot for the naphthalene PES of Cané et al.³⁷ Other details are as in Figure 2, except that the hole saddle point energy is now 2483.050 cm⁻¹ above the global minimum.

was increased beyond the first lattice hole point energy, up to a maximum $V_{\rm cut}$ value of 8432 cm⁻¹, without any new holes appearing. As this is beyond the range of most chemically relevant applications, it was deemed not necessary to push things any further. In any event, even this "heroic" calculation (for which $N \approx 32.3$ million) required only ~ 5 GB and 18 h on a single CPU core.

Finally, the formic acid dimer system is quite different from the others in that it represents (a) a highly anharmonic complex rather than a molecule, (b) isomerization rather than dissociation, and (c) a legitimate saddle point rather than a hole. It thus provides a highly important test case for the *Crystal* method, even though the isomerization saddle point for the Qu and Bowman PES is of course already well-known. Note that the minimum and transition state structures have C_{2h} and D_{2h} point group symmetry, respectively; however, we did not exploit symmetry at all in our calculation (though we did presume a planar form).

Starting from one of the two equivalent PES minima, and using Cartesian coordinates with lattice spacings based on displacements relative to the other minimum, Crystal located a lattice hole point between $V_{\rm cut}$ values of 3958.42 and 3958.45 cm⁻¹. The largest $V_{\rm cut1}$ calculation required $N \approx 338084$ grid points and ~33 min on a single Quanah CPU core. Starting from the lattice hole point, gradient norm minimization, etc., were then used to locate the isomerization saddle point. The resultant energy (i.e., 2847.55 cm⁻¹ above the minimum) agrees perfectly with that reported in the original study.³⁹

In conclusion, (a) explicit PES functions, obtained as automated fits or interpolations of *ab initio* data, will play an important role in the future of dynamics, even for large systems. (b) In this milieu, PES holes are a tremendous nuisance, becoming increasingly difficult to both avoid and detect. Legitimate saddle points are also much harder to find. (c) *Crystal* provides an accurate, inexpensive, reliable, and automated tool, for identifying PES holes and legitimate saddle points, and determining their precise locations. (d) *Crystal* also provides a "hole plugging" feature, allowing users to locate multiple saddle points, in energetic order (e.g., prior to modifying or "fixing" PESs, in the case of holes). (e) The latest *Crystal* source code and user's manual are always available from the authors on request.

ASSOCIATED CONTENT

Supporting Information

The Supporting Information is available free of charge at https://pubs.acs.org/doi/10.1021/acs.jpclett.0c01435.

Tables of normal modes and their frequencies for uracil and naphthalene and tables of lowest-lying lattice hole point and hole saddle point geometries for uracil and naphthalene (PDF)

AUTHOR INFORMATION

Corresponding Author

Bill Poirier — Department of Chemistry and Biochemistry, Texas Tech University, Lubbock, Texas 79409-1061, United States; orcid.org/0000-0001-8277-746X; Phone: 806-834-3099; Email: bill.poirier@ttu.edu; Fax: 806-742-1289

Author

Ankit Pandey — Department of Chemistry and Biochemistry, Texas Tech University, Lubbock, Texas 79409-1061, United States

Complete contact information is available at: https://pubs.acs.org/10.1021/acs.jpclett.0c01435

Notes

The authors declare no competing financial interest.

ACKNOWLEDGMENTS

This work was largely supported by a grant from The Robert A. Welch Foundation (D-1523). In addition, both a research grant (CHE-1665370) and a CRIF MU instrumentation grant (CHE-0840493) from the National Science Foundation are acknowledged. The authors also gratefully acknowledge the Texas Tech University High Performance Computing Center for providing access and technical support to their Quanah computing cluster facility. This article is dedicated to the memory of Prof. William L. Hase.

REFERENCES

- (1) Miller, W. H. The Semiclassical Initial Value Representation: A Potentially Practical Way for Adding Quantum Effects to Classical Molecular Dynamics Simulations. *J. Phys. Chem. A* **2001**, *105*, 2942.
- (2) Römer, S.; Burghardt, I. Towards a variational formulation of mixed quantum-classical molecular dynamics. *Mol. Phys.* **2013**, *111*, 3618–3624.
- (3) Richardson, J. O.; Althorpe, S. C. Ring-polymer instanton method for calculating tunneling splittings. *J. Chem. Phys.* **2011**, *134*, 054109.
- (4) Pratihar, S.; Ma, X.; Homayoon, Z.; Barnes, G. L.; Hase, W. L. Direct Chemical Dynamics Simulations. *J. Am. Chem. Soc.* **2017**, *139*, 3570–3590
- (5) Ischtwan, J.; Collins, M. A. Molecular Potential Energy Surfaces by Interpolation. *J. Chem. Phys.* **1994**, *100*, 8080–8088.
- (6) Quintas-Sánchez, E.; Dawes, R. AUTOSURF: A freely available program to construct potential energy surfaces. *J. Chem. Inf. Model.* **2019**, *59*, 262–271.
- (7) Győri, T.; Czakó, G. Automating the Development of High-Dimensional Reactive Potential Energy Surfaces with the ROBO-SURFER Program System. *J. Chem. Theory Comput.* **2020**, *16*, 51–66.
- (8) Behler, J.; Parrinello, M. Generalized neural-network representation of high-dimensional potential-energy surfaces. *Phys. Rev. Lett.* **2007**, *98*, 146401.
- (9) Manzhos, S.; Carrington, T., Jr Using neural networks to represent potential surfaces as sums of products. *J. Chem. Phys.* **2006**, *125*, 194105.
- (10) Jiang, B.; Guo, H. Permutation Invariant Polynomial Neural Network Approach to Fitting Potential Energy Surfaces. *J. Chem. Phys.* **2013**, *139*, 054112.
- (11) Petty, C.; Spada, R. F. K.; Machado, F. B. C.; Poirier, B. Accurate rovibrational energies of ozone isotopologues up to J = 10 utilizing artificial neural networks. *J. Chem. Phys.* **2018**, *149*, 024307.
- (12) Maeda, S.; Ohno, K.; Morokuma, K. Systematic exploration of the mechanism of chemical reactions: the global reaction route mapping (GRRM) strategy using the ADDF and AFIR methods. *Phys. Chem. Chem. Phys.* **2013**, *15*, 3683–3701.
- (13) Ohno, K.; Maeda, S. A scaled hypersphere search method for the topography of reaction pathways on the potential energy surface. *Chem. Phys. Lett.* **2004**, 384, 277–282.
- (14) Maeda, S.; Watanabe, Y.; Ohno, K. Finding important anharmonic terms in the sixth-order potential energy function by the scaled hypersphere search method: An application to vibrational analyses of molecules and clusters. J. Chem. Phys. 2008, 128, 144111.

- (15) Jensen, F. Introduction to Computational Chemistry; John Wiley and Sons: Chichester, U.K., 1999.
- (16) Henkelman, G.; Jónsson, H. Improved tangent estimate in the nudged elastic band method for finding minimum energy paths and saddle points. *J. Chem. Phys.* **2000**, *113*, 9978–9985.
- (17) Halgren, T. A.; Lipscomb, W. N. The synchronous-transit method for determining reaction pathways and locating molecular transition states. *Chem. Phys. Lett.* **1977**, 49, 225–232.
- (18) Dewar, M. J. S.; Healy, E. F.; Stewart, J. J. P. Location of transition states in reaction mechanisms. *J. Chem. Soc., Faraday Trans.* 2 **1984**, *80*, 227–233.
- (19) Banerjee, A.; Adams, N.; Simons, J.; Shepard, R. Search for stationary points on surfaces. *J. Phys. Chem.* **1985**, *89*, 52–57.
- (20) Cerjan, C. J.; Miller, W. H. On finding transition states. *J. Chem. Phys.* **1981**, *75*, 2800.
- (21) Császár, C.; Pulay, P. Geometry optimization by direct inversion in the iterative subspace. *J. Mol. Struct.* **1984**, *114*, 31–34.
- (22) Abashkin, Y.; Russo, N. Transition state structures and reaction profiles from constrained optimization procedure. Implementation in the framework of density functional theory. *J. Chem. Phys.* **1994**, *100*, 4477.
- (23) Xiao, H.-Y.; Maeda, S.; Morokuma, K. Excited-State Roaming Dynamics in Photolysis of a Nitrate Radical. *J. Phys. Chem. Lett.* **2011**, 2, 934–938.
- (24) Grubb, M. P.; Warter, M. L.; Xiao, H.; Maeda, S.; Morokuma, K.; North, S. W. No Straight Path: Roaming in Both Ground- and Excited-State Photolytic Channels of NO3 \rightarrow NO + O2. *Science* **2012**, 335, 1075–1078.
- (25) Halverson, T.; Poirier, B. Accurate quantum dynamics calculations using symmetrized Gaussians on a doubly dense Von Neumann lattice. *J. Chem. Phys.* **2012**, *137*, 224101.
- (26) Pandey, A.; Poirier, B. An algorithm to find (and plug) "holes" in multi-dimensional surfaces. *J. Chem. Phys.* **2020**, *152*, 214102.
- (27) Thomas, P. S.; Carrington, T.; Agarwal, J.; Schaefer, H. F., III Using an iterative eigensolver and intertwined rank reduction to compute vibrational spectra of molecules with more than a dozen atoms: Uracil and naphthalene. *J. Chem. Phys.* **2018**, *149*, 064108.
- (28) Ohno, K.; Maeda, S. Ab initio anharmonic calculations of vibrational frequencies of benzene by means of efficient construction of potential energy functions. *Chem. Phys. Lett.* **2011**, 503, 322–326.
- (29) Liotard, D.; Rérat, M. Equivariant Morse theory of the N-body problem: Application to potential surfaces in chemistry. *Theoretica Chimica Acta* **1993**, *86*, 297–313.
- (30) Pandey, A.; Poirier, B. Using phase-space Gaussians to compute the vibrational states of OCHCO⁺. *J. Chem. Phys.* **2019**, *151*, 014114.
- (31) Holley, R. W.; Apgar, J.; Everett, G. A.; Madison, J. T.; Marquisee, M.; Merrill, S. H.; Penswick, J. R.; Zamir, A. Structure of a Ribonucleic Acid. *Science* **1965**, *147*, 1462.
- (32) Krasnoshchekov, S. V.; Vogt, N.; Stepanov, N. F. Ab Initio Anharmonic Analysis of Vibrational Spectra of Uracil Using the Numerical-Analytic Implementation of Operator Van Vleck Perturbation Theory. *J. Phys. Chem. A* **2015**, *119*, 6723.
- (33) Maslen, P. E.; Handy, N. C.; Amos, R. D.; Jayatilaka, D. Higher analytic derivatives. IV. Anharmonic effects in the benzene spectrum. *J. Chem. Phys.* **1992**, *97*, 4233–4254.
- (34) Halverson, T.; Poirier, B. One Million Quantum States of Benzene. J. Phys. Chem. A 2015, 119, 12417–12433.
- (35) Ceotto, M.; Di Liberto, G.; Conte, R. Semiclassical "Divideand-Conquer" Method for Spectroscopic Calculations of High Dimensional Molecular Systems. *Phys. Rev. Lett.* **2017**, *119*, 010401.
- (36) Parker, D. S. N.; Zhang, F.; Kim, Y. S.; Kaiser, R. I.; Landera, A.; Kislov, V. V.; Mebel, A. M.; Tielens, A. G. G. M. Low temperature formation of naphthalene and its role in the synthesis of PAHs (Polycyclic Aromatic Hydrocarbons) in the interstellar medium. *Proc. Natl. Acad. Sci. U. S. A.* **2012**, *109*, 53–58.
- (37) Cané, E.; Miani, A.; Trombetti, A. Anharmonic Force Fields of Naphthalene- h_8 and Naphthalene- d_8 . *J. Phys. Chem. A* **2007**, 111, 8218.

- (38) Balabin, R. M. Polar (Acyclic) Isomer of Formic Acid Dimer: Gas-Phase Raman Spectroscopy Study and Thermodynamic Parameters. *J. Phys. Chem. A* **2009**, *113*, 4910–4918.
- (39) Qu, C.; Bowman, J. M. An ab initio potential energy surface for the formic acid dimer: zero-point energy, selected anharmonic fundamental energies, and ground-state tunneling splitting calculated in relaxed 1–4-mode subspaces. *Phys. Chem. Chem. Phys.* **2016**, *18*, 24835–24840.
- (40) Puzzarini, C.; Biczysko, M.; Barone, V. Accurate Anharmonic Vibrational Frequencies for Uracil: The Performance of Composite Schemes and Hybrid CC/DFT Model. *J. Chem. Theory Comput.* **2011**, *7*, 3702.